Supplementary Information

Earlier peak photosynthesis timing accelerates wildfire outbreak and expands burned area

Gengke Lai[1,2†], Jialing Li[1,2†], Jun Wang[3†], Chaoyang Wu[3]*, Yongguang Zhang[1,2,4,8]*, Constantin M. Zohner[5], Josep Peñuelas[6,7,8]

1. International Institute for Earth System Sciences, Jiangsu Center for Collaborative Innovation in Geographical Information Resource Development and Application, Nanjing University, Nanjing, Jiangsu, China;
2. Jiangsu Provincial Key Laboratory of Geographic Information Science and Technology, Key Laboratory for Land Satellite Remote Sensing Applications of Ministry of Natural Resources, School of Geography and Ocean Science, Nanjing University, Nanjing, Jiangsu 210023, China;
3. The Key Laboratory of Land Surface Pattern and Simulation, Institute of Geographical Sciences and Natural Resources Research, Chinese Academy of Sciences, Beijing, 100101, China;
4. Huangshan National Park Ecosystem Field Scientific Observation and Research Station of the Ministry of Education, Nanjing, Jiangsu 210023, China;
5. Department of Environmental Systems Science, Institute of Integrative Biology, ETH Zurich, Zurich, Switzerland.
6. CSIC, Global Ecology Unit CREAF-CSIC-UAB, Bellaterra, Barcelona 08193, Catalonia, Spain;
7. CREAF, Cerdanyola del Valles, Barcelona 08193, Catalonia, Spain;
8. International Joint Carbon Neutrality Laboratory, Nanjing University, Nanjing, Jiangsu 210023, China.

***Corresponding authors:** C Wu (wucy@igsnrr.ac.cn), Y Zhang (yongguang_zhang@nju.edu.cn). † equal contribution.

This supplementary file includes:

Supplementary Figures S1-S14 and Supplementary Tables S1-S2

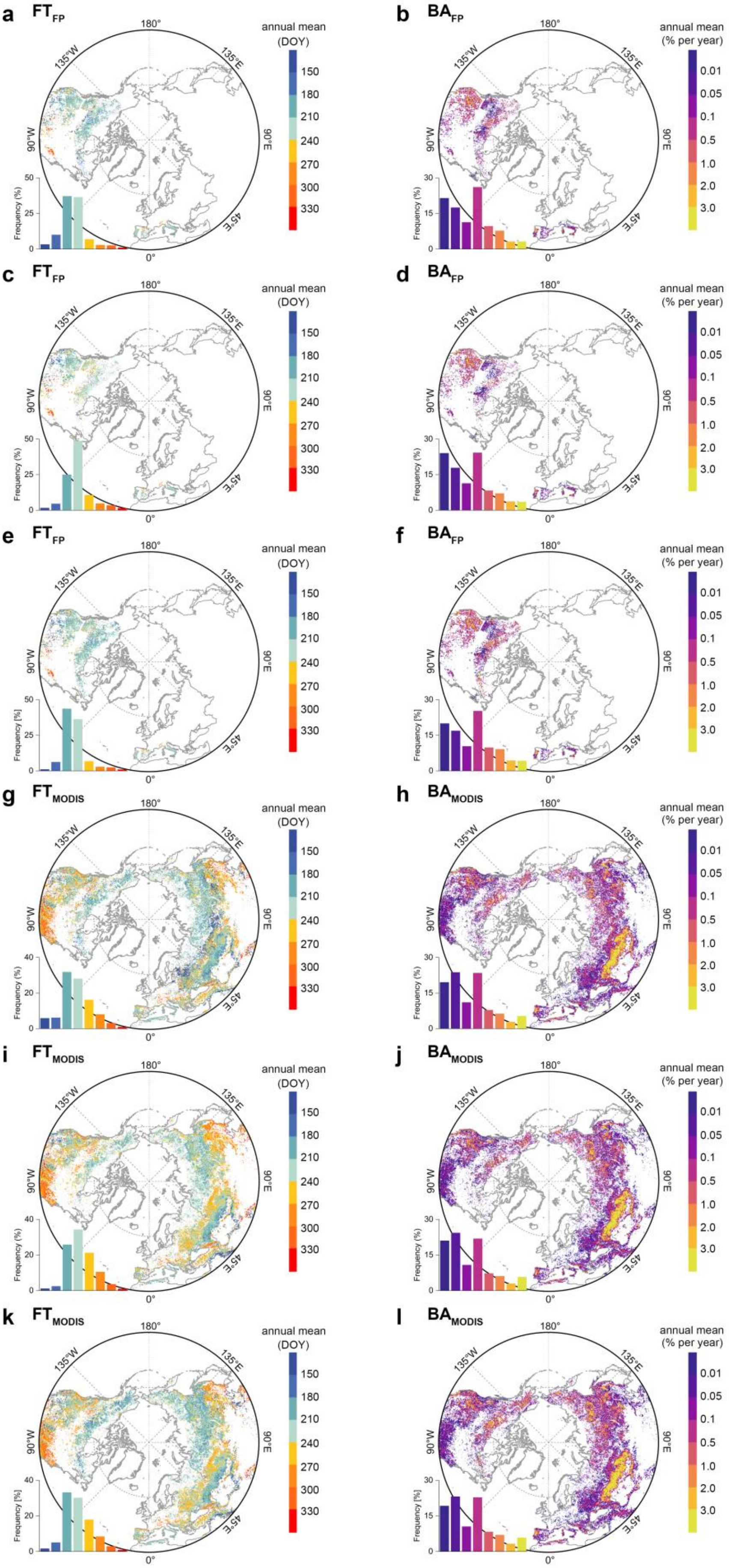
a FT$_{FP}$
b BA$_{FP}$
c FT$_{FP}$
d BA$_{FP}$
e FT$_{FP}$
f BA$_{FP}$
g FT$_{MODIS}$
h BA$_{MODIS}$
i FT$_{MODIS}$
j BA$_{MODIS}$
k FT$_{MODIS}$
l BA$_{MODIS}$
180°
135°W
135°E
90°W
90°E
45°E
0°
annual mean (DOY)
150
180
210
240
270
300
330
annual mean (% per year)
0.01
0.05
0.1
0.5
1.0
2.0
3.0
Frequency (%)
0
15
30
25
50
20
40

Figure S1 | Spatial patterns of annual means of wildfire outbreak (FT) and burned area (BA) after peak photosynthesis timing (PPT) derived from terrestrial fire perimeters (FP) and MODIS observations in northern ecosystems for 2001-2018. **a-b**, FT_{FP} and BA_{FP} after LT_SIFc derived PPT_{SIF}; **c-d**, FT_{FP} and BA_{FP} after PPT_{NDVI}; **e-f**, FT_{FP} and BA_{FP} after GOSIF derived PPT_{SIF}; **g-h**, FT_{MODIS} and BA_{MODIS} after LT_SIFc derived PPT_{SIF}; **i-j**, FT_{MODIS} and BA_{MODIS} after PPT_{NDVI}; **k-l**, FT_{MODIS} and BA_{MODIS} after GOSIF derived PPT_{SIF}.

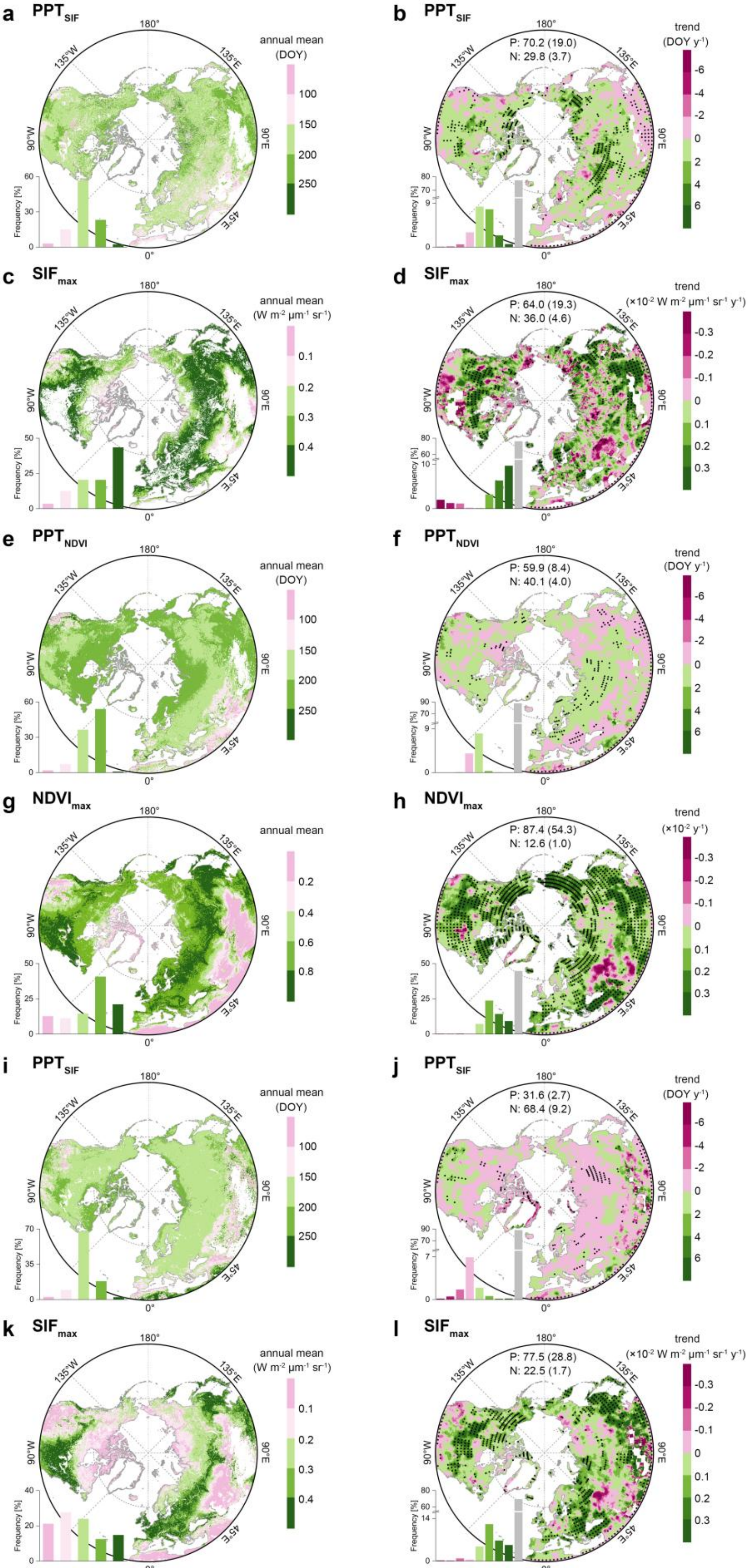
a PPT_SIF
annual mean (DOY)
100
150
200
250
b PPT_SIF
P: 70.2 (19.0)
N: 29.8 (3.7)
trend (DOY y-1)
-6
-4
-2
0
2
4
6
c SIF_max
annual mean (W m-2 μm-1 sr-1)
0.1
0.2
0.3
0.4
d SIF_max
P: 64.0 (19.3)
N: 36.0 (4.6)
trend (×10-2 W m-2 μm-1 sr-1 y-1)
-0.3
-0.2
-0.1
0
0.1
0.2
0.3
e PPT_NDVI
annual mean (DOY)
f PPT_NDVI
P: 59.9 (8.4)
N: 40.1 (4.0)
g NDVI_max
annual mean
0.2
0.4
0.6
0.8
h NDVI_max
P: 87.4 (54.3)
N: 12.6 (1.0)
trend (×10-2 y-1)
i PPT_SIF
annual mean (DOY)
j PPT_SIF
P: 31.6 (2.7)
N: 68.4 (9.2)
k SIF_max
annual mean (W m-2 μm-1 sr-1)
l SIF_max
P: 77.5 (28.8)
N: 22.5 (1.7)
180°
135°W
135°E
90°W
90°E
45°E
0°
Frequency [%]

Figure S2 | Spatial patterns of annual means and trends of the maximum photosynthesis and its timing (PPT) derived from LT_SIFc (a-d), NDVI (e-h), and GOSIF (i-l) products in northern ecosystems for 2001-2018. Black dots indicate the regions with significant trends (*p*-value<0.1). P and N indicate the percentage of increased and decreased trends, respectively. The long-term trend was calculated by the Mann-Kendall test and Theil-Sen slope estimator (MK-TS). We calculated the trend of centered grid cell after averaging values within a 9×9 spatial moving window (2.25°×2.25°).

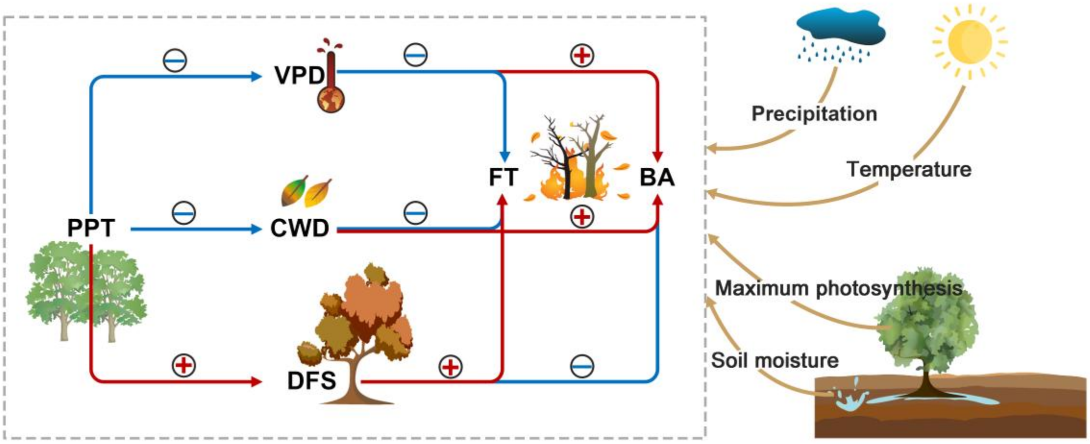

Figure S3 | Schematic path diagram showing the effect of peak photosynthesis timing on wildfire outbreak and burned area through changing atmospheric aridity (VPD), plant water stress (CWD), and leaf senescence (DFS). This path diagram contains three hypothetical pathways: PPT-VPD-wildfire, PPT-CWD-wildfire, and PPT-DFS-wildfire. The model also considers the effect of temperature, precipitation, maximum photosynthesis, and soil moisture. The + and – in circle indicate positive (red) and negative (blue) bivariate correlation, respectively. PPT: peak photosynthesis timing; VPD: vapor pressure deficit; CWD: climatic water deficit; DFS: date of autumn foliar senescence; FT: fire timing after PPT; BA: burned area after PPT.

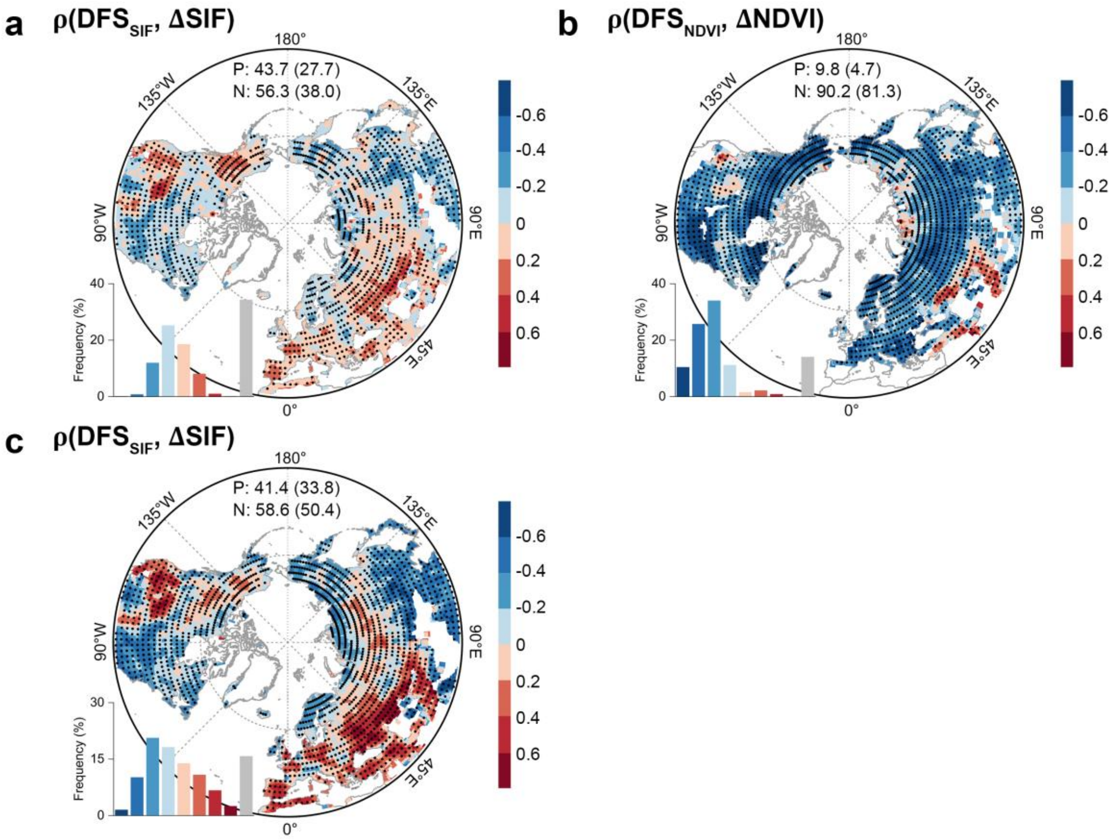

Figure S4 | The Spearman correlation between DFS and ΔSIF/ΔNDVI for LT_SIFc (a), NDVI (b), and GOSIF (c). We used ΔSIF/ΔNDVI to represent the accumulated dead fuels induced by leaf senescence. ΔSIF/ΔNDVI was calculated as the monthly difference of SIF/NDVI from July to October (representing the entire senescence period[1]). It showed that DFS was negatively correlated with ΔSIF/ΔNDVI, which suggested that the earlier DFS leads to the enhancement of dead litters over the senescence period. Black dots indicate the regions with significant correlations (*p*-value<0.1).

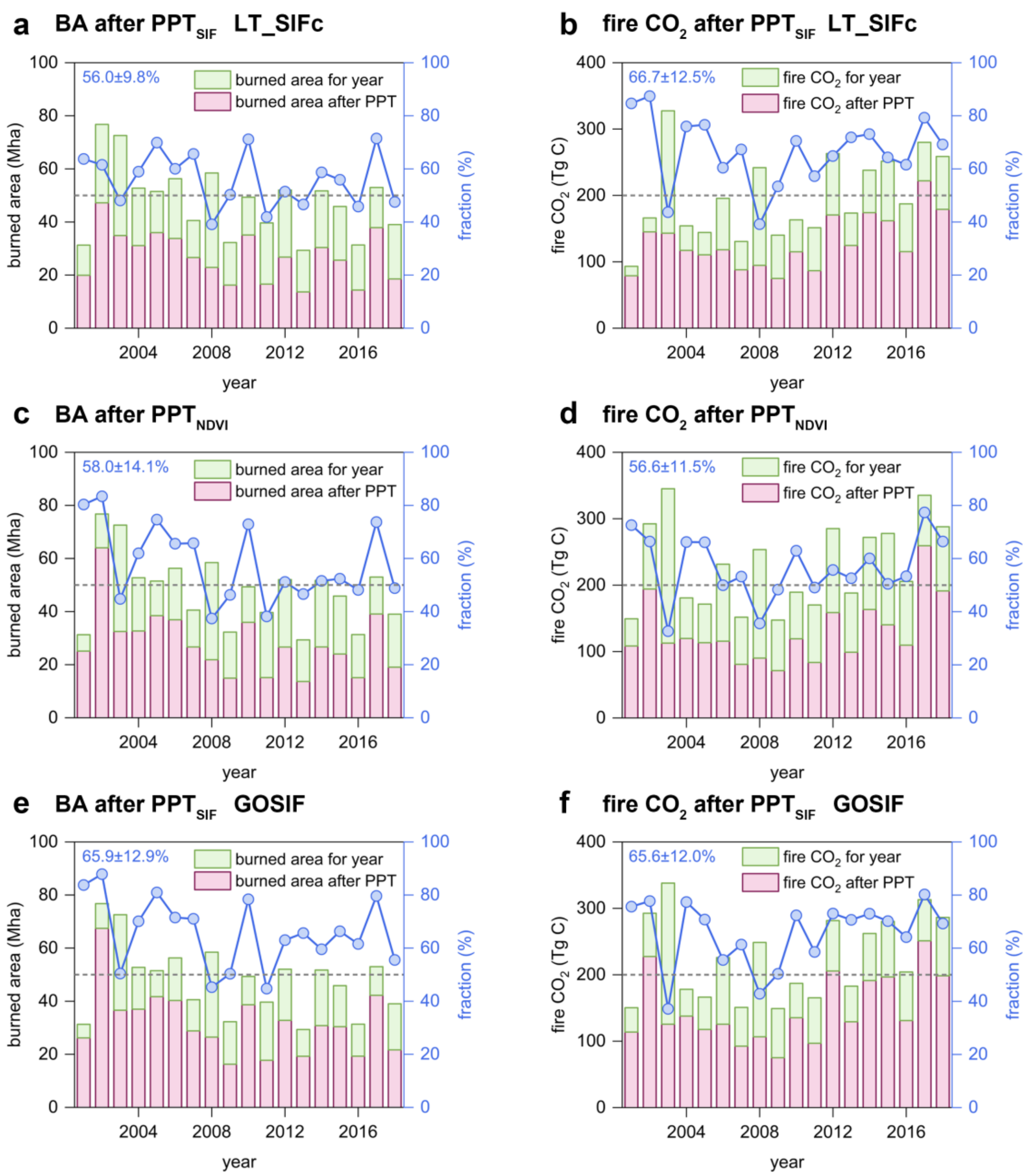

Figure S5 | Annual fractions (blue lines) of burned area and wildfire CO_2 emission after peak photosynthesis timing (red bars) in relative to the annual total (green bars) in northern ecosystems (>30°N) for LT_SIFc (a-b), NDVI (c-d), and GOSIF (e-f). The blue label indicates the annual mean ± standard deviation of the fraction. The gray dotted line indicates the 50% fraction. The CO_2 emission was derived from the global fire CO_2 emission dataset[2].

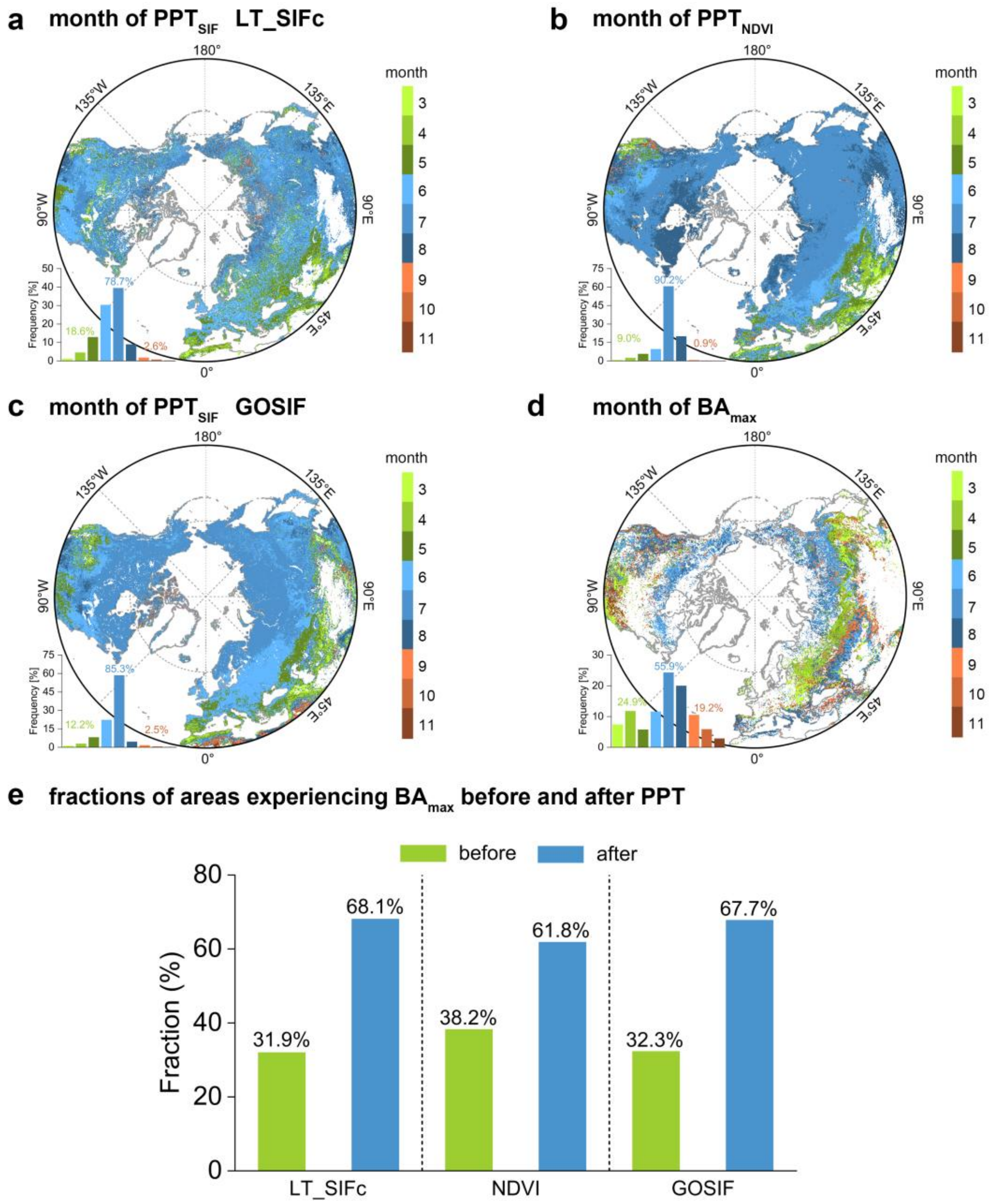

Figure S6 | Comparisons between the months of peak photosynthesis timing and maximal fire activity. Spatial patterns of the months of PPT derived from LT_SIFc (**a**), NDVI (**b**), and GOSIF (**c**), and maximal burned area (BA_{max}, **d**). The color labels in the bottom left indicate the fractions of months in spring (green), summer (blue), and autumn (orange). **e**, the fractions of pixels experiencing BA_{max} before and after PPT derived from LT_SIFc, NDVI, and GOSIF.

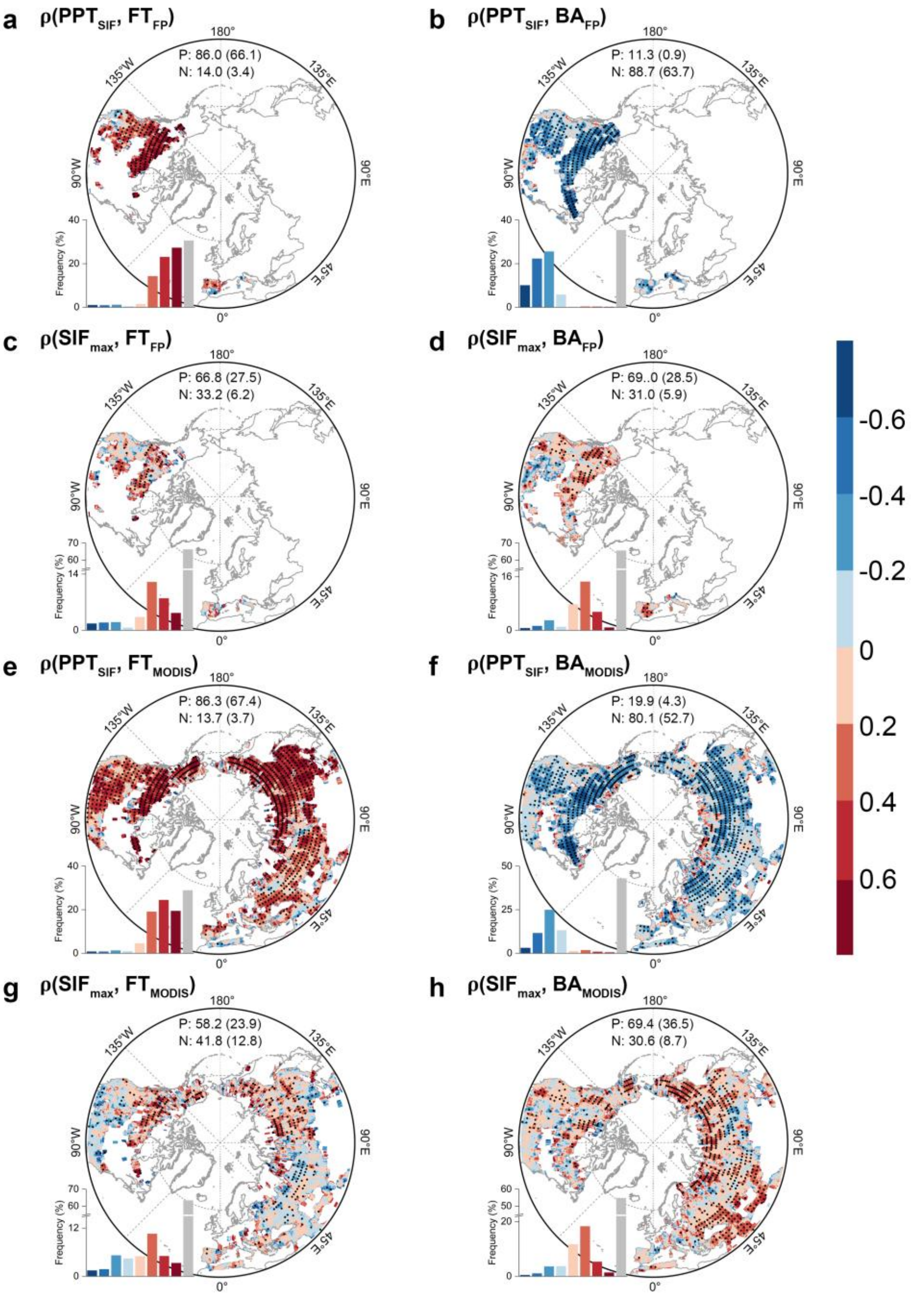

Figure S7 | Controls of peak vegetation growth derived from GOSIF on wildfire outbreak and burned area in northern ecosystems (>30°N). Partial correlations (ρ) between PPT_{SIF}/SIF_{max} and FT/BA for terrestrial fire perimeters (**a-d**) and MODIS (**e-h**) observations. Black dots indicate the regions with significant correlations (*p*-value<0.1). In summary, our results were robust that PPT positively correlated with wildfire timing but had a negative relationship with burned area.

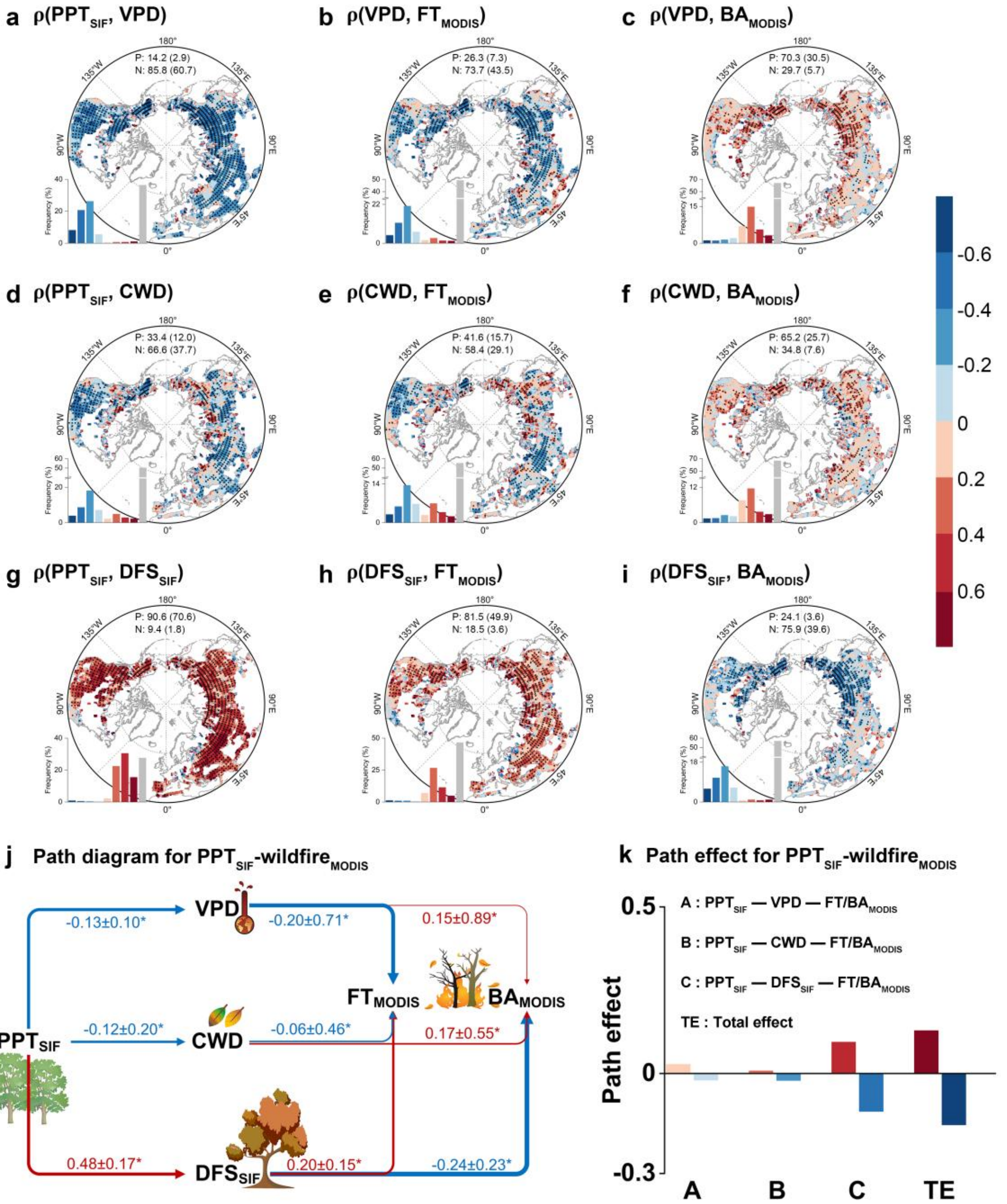

Figure S8 | Potential mechanisms underlying the linkage between MODIS derived wildfire activity and GOSIF derived peak photosynthesis timing. a-i, Spatial patterns of partial correlations for PPT$_{SIF}$-VPD-wildfire (**a-c**), PPT$_{SIF}$-CWD-wildfire (**d-f**), and PPT$_{SIF}$-DFS$_{SIF}$-wildfire (**g-i**). Black dots indicate the regions with significant partial correlations (p-value<0.1). **j-k**, Path diagram (**j**) and path effect (**k**) for PPT$_{SIF}$-wildfire$_{MODIS}$. The numbers in the path diagram represent the mean and standard deviation of standardized path coefficients across the northern ecosystems (>30°N), asterisks indicate the path coefficients are significant (p-value<0.1) and the colors (red and blue arrows represent positive and negative effects, respectively) and widths of the arrows represent the signs and magnitudes of the path coefficients, respectively. Red and blue bars represent path effects for PPT-FT and PPT-BA, respectively. In summary, our results were robust that PPT amplified wildfire activities through increasing VPD and CWD, and advancing DFS.

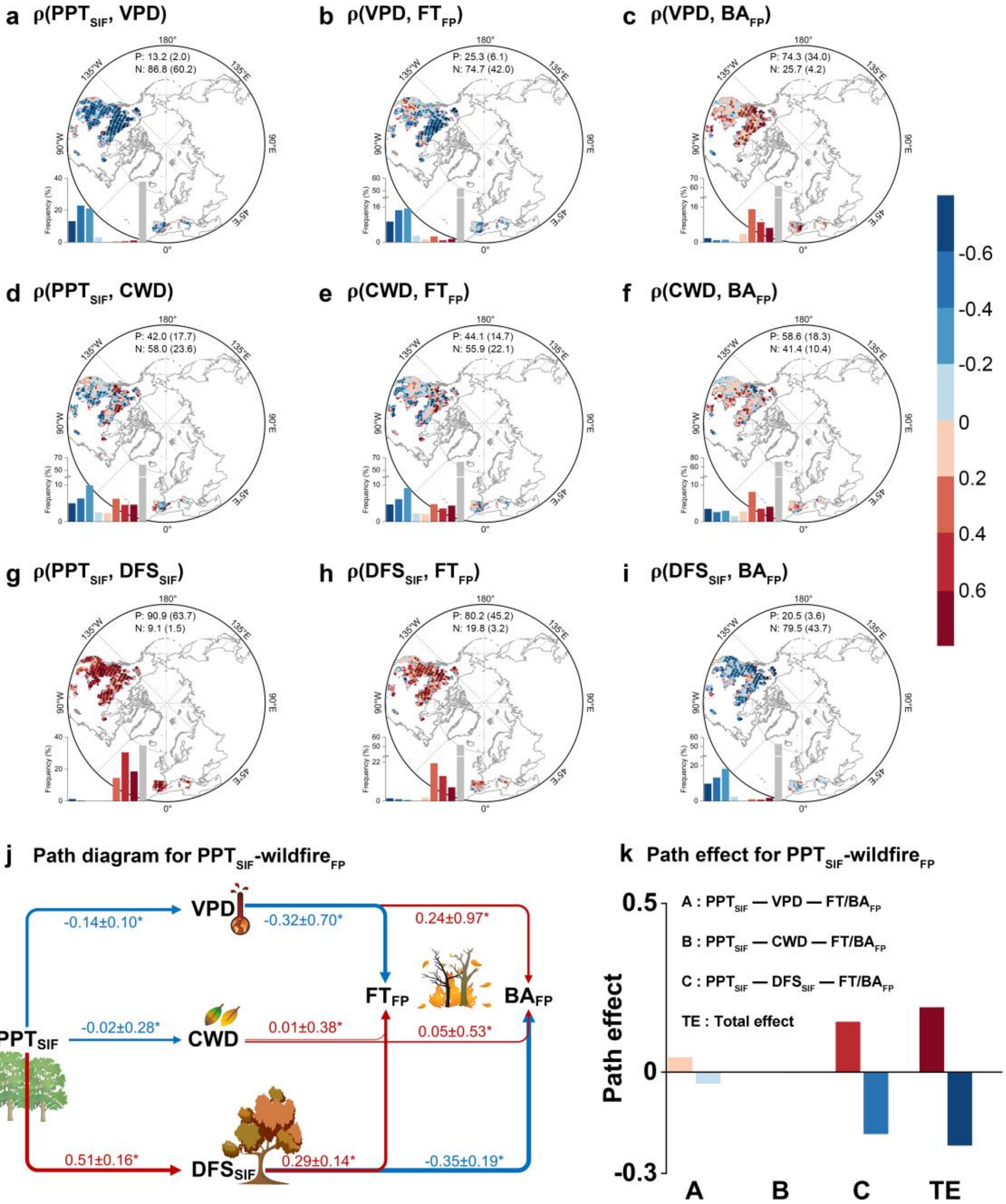

Figure S9 | Potential mechanisms underlying the linkage between FP derived wildfire activity and GOSIF derived peak photosynthesis timing. a-i, Spatial patterns of partial correlations for PPT_{SIF}-VPD-wildfire (**a-c**), PPT_{SIF}-CWD-wildfire (**d-f**), and PPT_{SIF}-DFS_{SIF}-wildfire (**g-i**). Black dots indicate the regions with significant partial correlations (*p*-value<0.1). **j-k**, Path diagram (**j**) and path effect (**k**) for PPT_{SIF}-$wildfire_{FP}$. The numbers in the path diagram represent the mean and standard deviation of standardized path coefficients across the northern ecosystems (>30°N), asterisks indicate the path coefficients are significant (p-value<0.1) and the colors (red and blue arrows represent positive and negative effects, respectively) and widths of the arrows represent the signs and magnitudes of the path coefficients, respectively. Red and blue bars represent path effects for PPT-FT and PPT-BA, respectively. In summary, our results were robust that PPT amplified wildfire activities through increasing VPD and CWD, and advancing DFS.

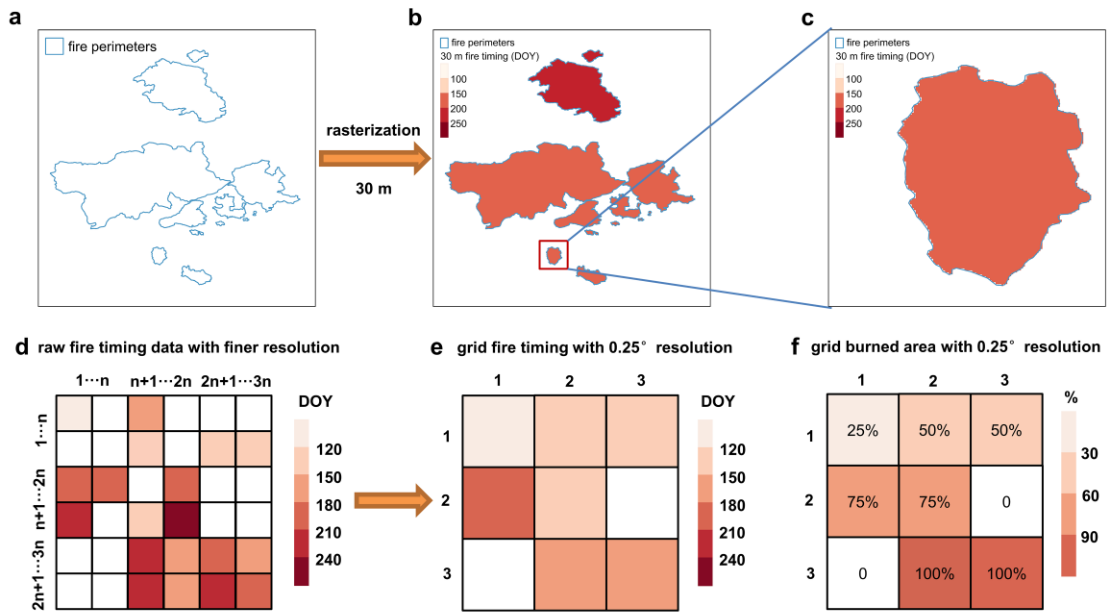

Figure S10 | Schematic of the processing of terrestrial fire perimeters (a-c) and the calculations of fire timing (FT) and burned area (BA) from finer resolution to 0.25° grid cell (d-f). a-c suggested that a 0.00025° (approximately 30 m) resolution can match fire perimeters well. **d-f** showed that FT and BA were identified as the date (DOY) of the first wildfire outbreak (the lightest color) and total areas burned (showed as the percentage of burned pixels) after PPT, respectively. The size of pixel in **d** is 30×30 m for terrestrial fire perimeters and 500×500 m for MODIS product. A 0.25°×0.25° grid cell contains 1000×1000 30 m pixels or 60×60 500 m pixels. n=1000 for fire perimeters and n=60 for MODIS. The size of grid in **e** and **f** is 0.25°.

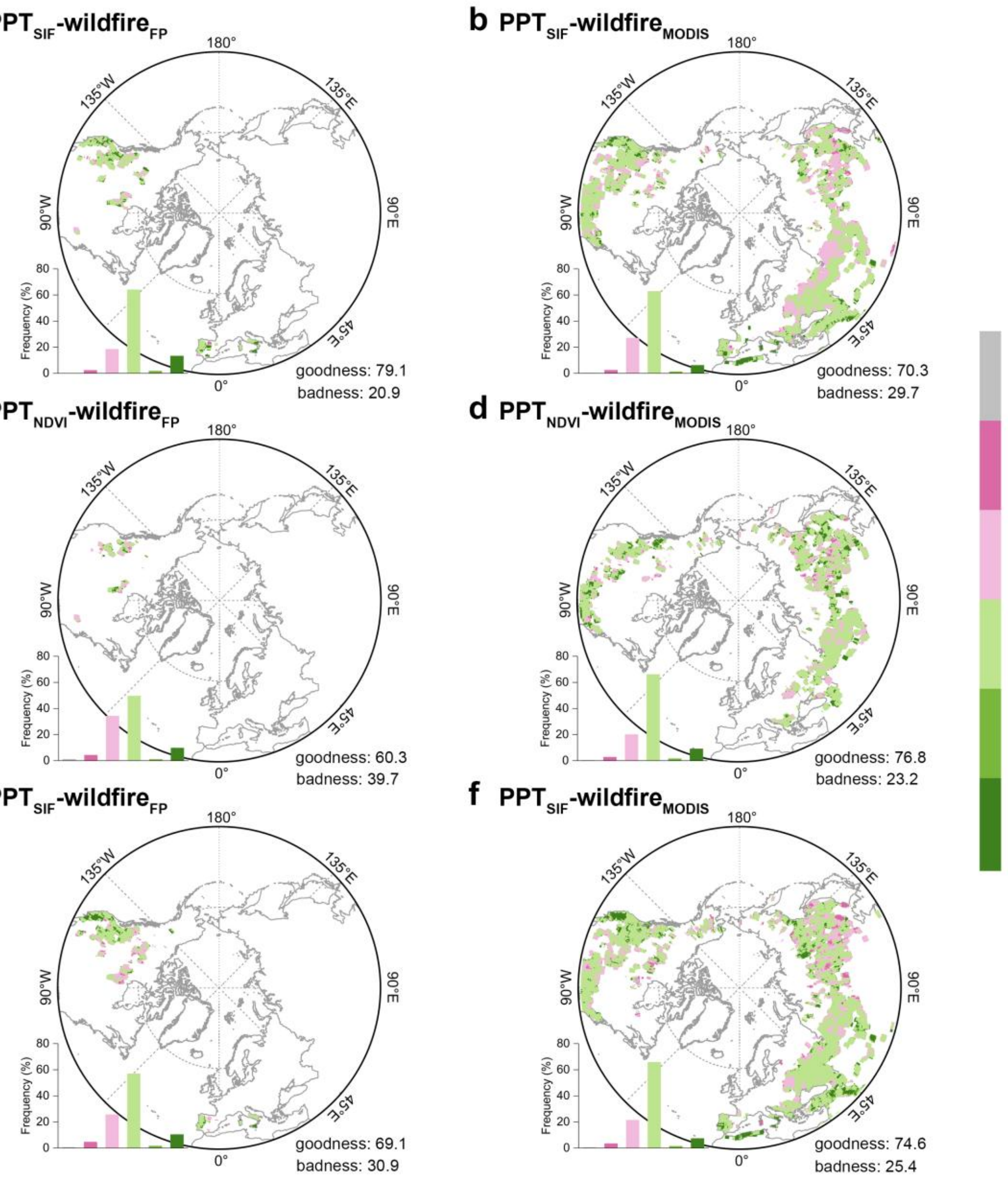

Figure S11 | Goodness of fit of the model using path analysis for LT_SIFc (a-b), NDVI (c-d), and GOSIF (e-f). We selected five metrics to evaluate the goodness of fitted model, i.e., GFI, CFI, RMSEA, NNFI, and SRMR. 0-5 indicate the number of criteria satisfied, and the model was considered reliable when three out of five criteria are met (green).

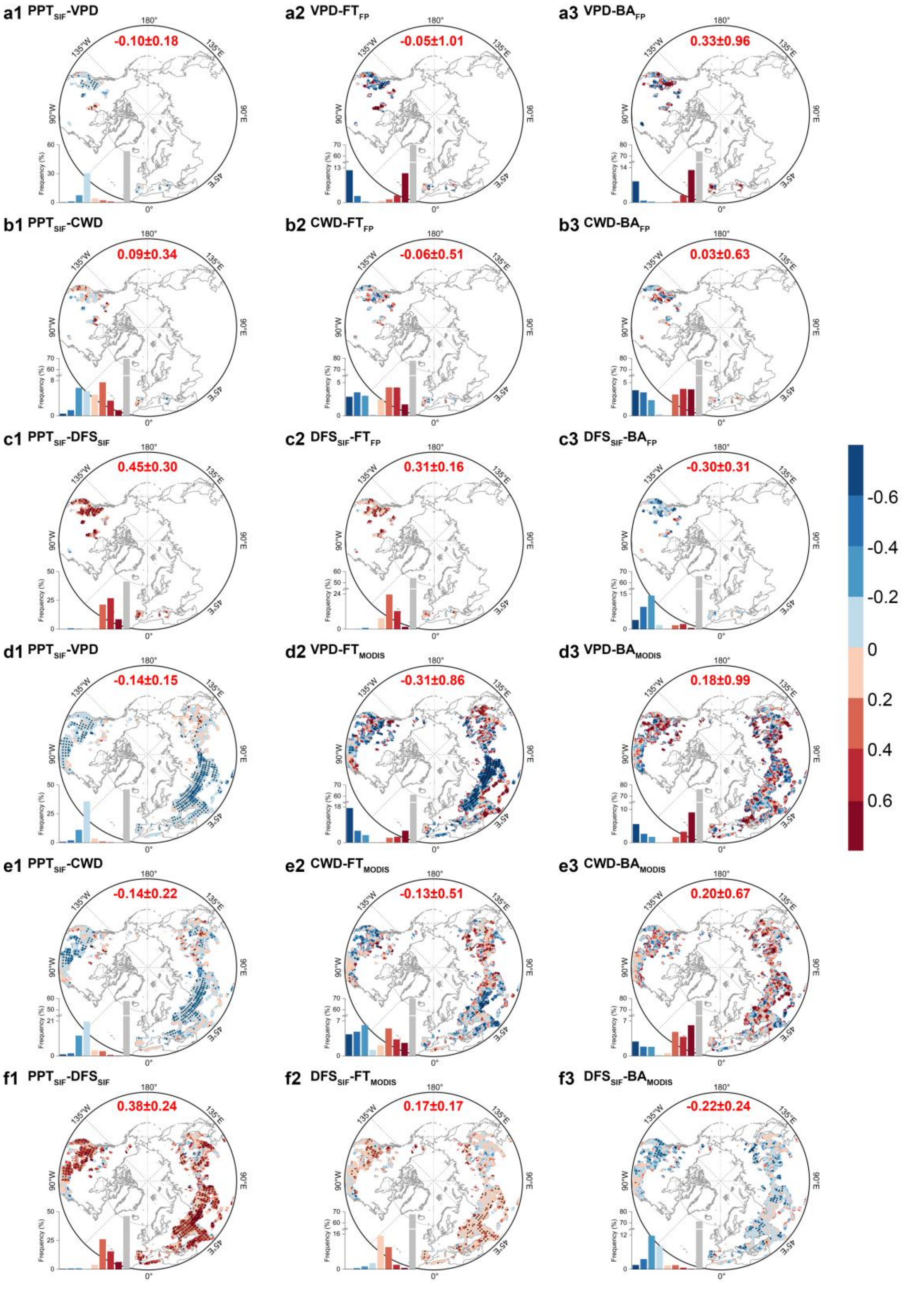

Figure S12 | Standard path coefficient of each path for LT_SIFc product. a-f indicate the VPD, CWD, and DFS_{SIF} pathways for terrestrial fire perimeters and MODIS products, respectively. **1-3** indicate the PPT_{SIF}-factor, factor-FT, and factor-BA, respectively. "*X*-*Y*" indicates the effect of *X* on *Y*. Black dot indicates the standard path coefficient is significant (*p*-value<0.1). Red label indicates the regional mean ± standard deviation of path coefficient considering the goodness of fit of the model and the significance of path coefficient.

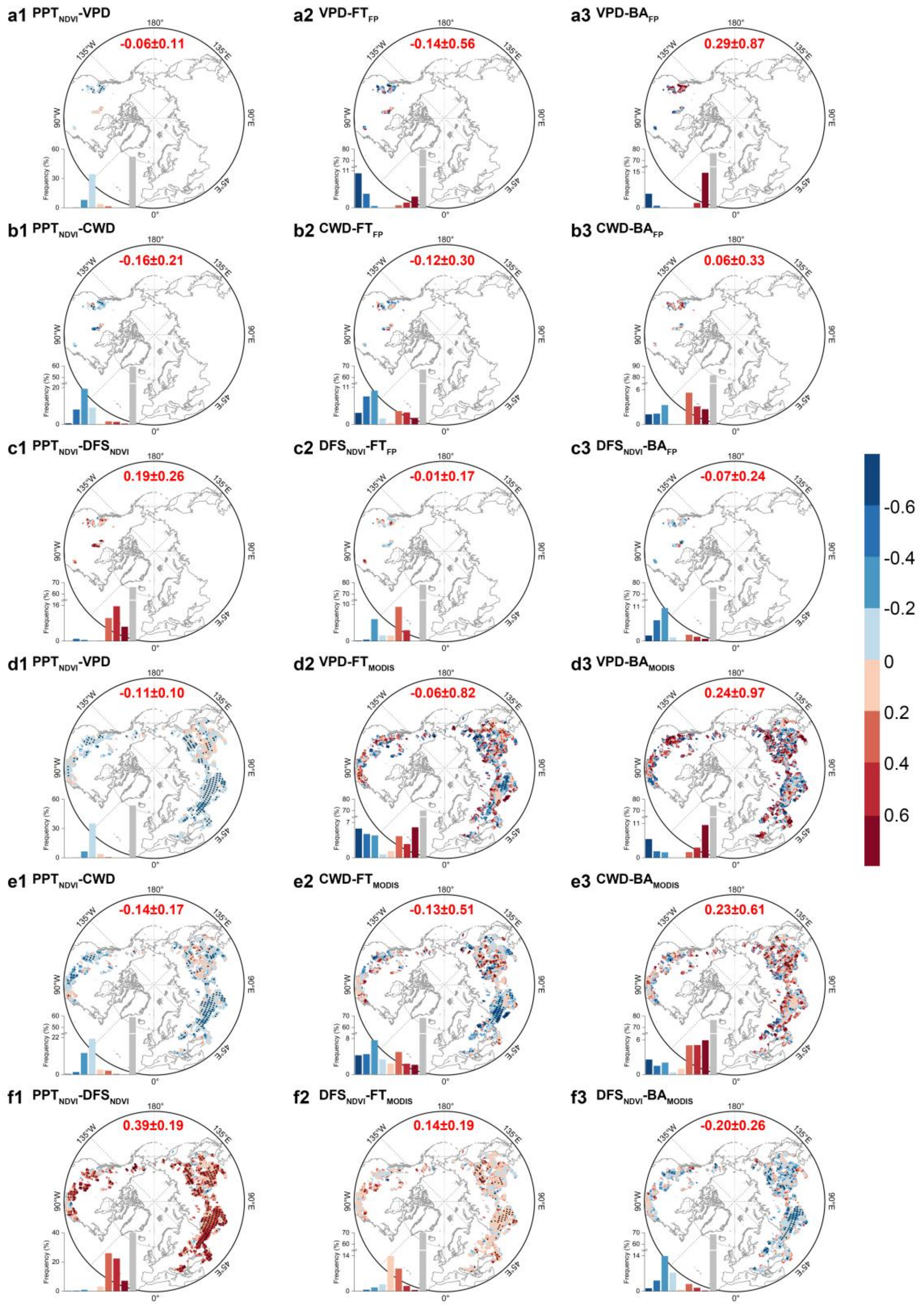

Figure S13 | Standard path coefficient of each path for NDVI product. a-f indicate the VPD, CWD, and DFS_{NDVI} pathways for terrestrial fire perimeters and MODIS products, respectively. **1-3** indicate the PPT_{NDVI}-factor, factor-FT, and factor-BA, respectively. "*X*-*Y*" indicates the effect of *X* on *Y*. Black dot indicates the standard path coefficient is significant (*p*-value<0.1). Red label indicates the regional mean ± standard deviation of path coefficient considering the goodness of fit of the model and the significance of path coefficient.

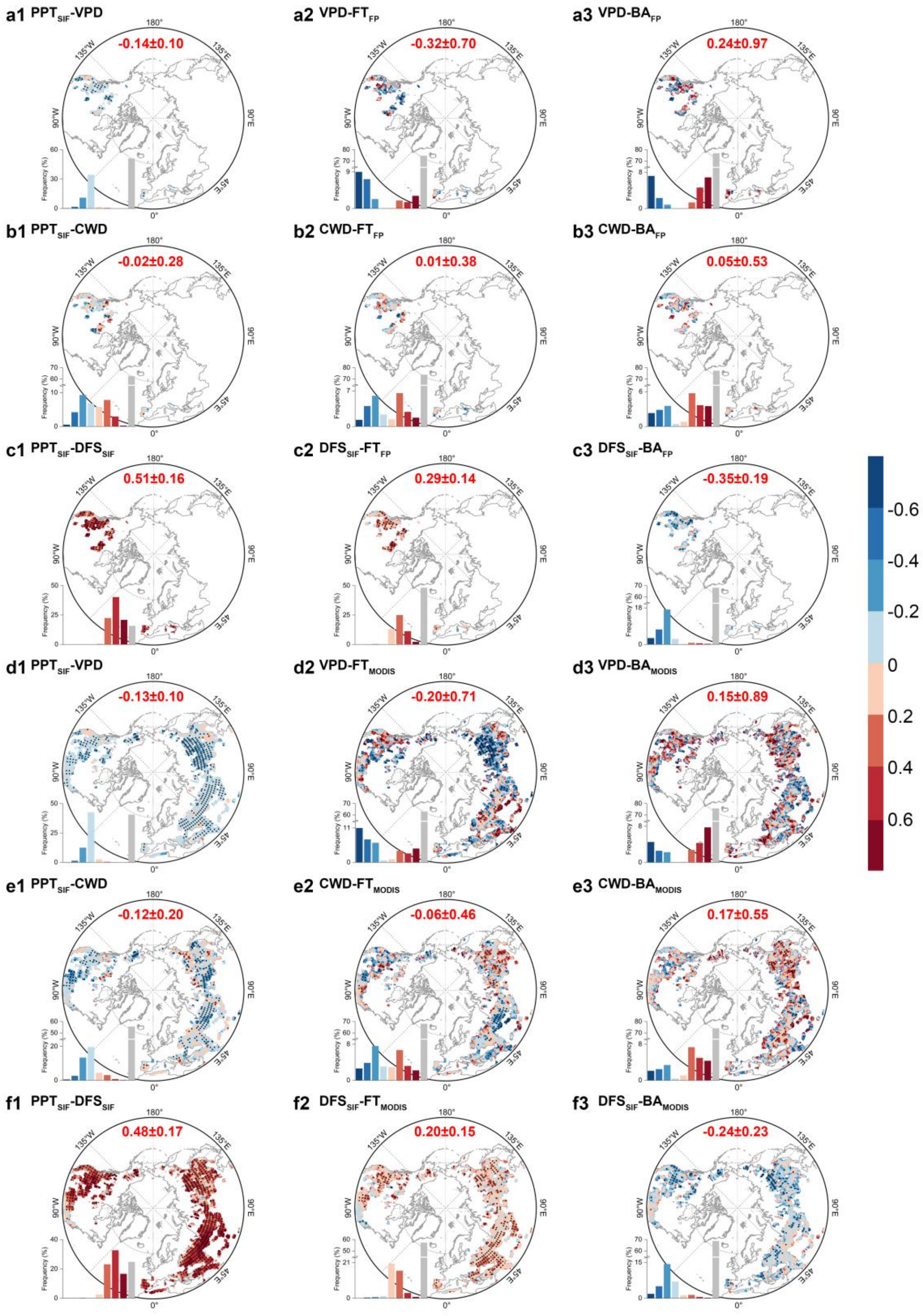

Figure S14 | Standard path coefficient of each path for GOSIF product. a-f indicate the VPD, CWD, and DFS_{SIF} pathways for terrestrial fire perimeters and MODIS products, respectively. **1-3** indicate the PPT_{SIF}-factor, factor-FT, and factor-BA, respectively. "X-Y" indicates the effect of X on Y. Black dot indicates the standard path coefficient is significant (*p*-value<0.1). Red label indicates the regional mean ± standard deviation of path coefficient considering the goodness of fit of the model and the significance of path coefficient.

Table S1 Summary of the data used in this study

Dataset	Indicator	Resolution	Period	Source
MOD13C1 V6	NDVI	0.05°, 16-day	2001-2018	https://lpdaac.usgs.gov/products/mod13c1v006/
LT_SIFc	SIF	0.05°, monthly	2001-2018	https://doi.org/10.6084/m9.figshare.21546066.v1
GOSIF		0.05°, 8-day	2001-2018	http://data.globalecology.unh.edu/data/GOSIF_v2/
NBAC	FT, BA	shapefile	2001-2018	https://cwfis.cfs.nrcan.gc.ca/datamart
MTBS		shapefile	2001-2018	https://www.mtbs.gov/direct-download
EFFIS		shapefile	2001-2018	https://effis.jrc.ec.europa.eu/applications/data-and-services
MCD64A1 V6		500 m, monthly	2001-2018	https://lpdaac.usgs.gov/products/mcd64a1v006/
ERA5-Land	T, PRE, SM, Td	0.1°, monthly	2001-2018	https://cds.climate.copernicus.eu/cdsapp#!/home
TerraClimate	CWD	1/24°, monthly	2001-2018	https://www.climatologylab.org/terraclimate.html
Vegetation photosynthetic phenology dataset	DFS	0.05°, yearly	2001-2018	https://doi.org/10.6084/m9.figshare.17195009.v3
MCD12Q1 V6	Landcover type	500 m, yearly	2001-2018	https://lpdaac.usgs.gov/products/mcd12q1v006/

GlobalFire CO_2	Global fire CO_2 emissions	3.75°×1.9°, monthly	2001-2018	https://figshare.com/articles/dataset/Global_fire_CO2_emissions_2000-2021/21770624

NDVI: normalized difference vegetation index; SIF: solar-induced chlorophyll fluorescence; FT: fire timing; BA: burned area; T: 2 m air temperature; PRE: total precipitation; SM: soil moisture; Td: 2 m dewpoint temperature; CWD: climatic water deficit; DFS: date of autumn foliar senescence. Notable, vapor pressure deficit (VPD) was calculated by T and Td from ERA5-Land products[3].

Table S2 Summary of the outputs of FireMIP fire-vegetation models[4,5] used in this study

Model	Resolution	Period	Output
CLM[6]	2.5°×1.875°, monthly	2001-2012	GPP, BF
JSBACH-SPITFIRE[7]	1.875°×1.875°, monthly	2001-2012	GPP, BF
LPJ-GUESS-SPITFIRE[8]	0.5°×0.5°, monthly	2001-2012	GPP, BF
ORCHIDEE-SPITFIRE[9]	0.5°×0.5°, monthly	2001-2012	GPP, BF
CTEM[10]	2.8125°×2.8125°, monthly	2001-2012	GPP, BF
JULES-INFERNO[11]	1.875°×1.245°, monthly	2001-2012	GPP, BF
LPJ-GUESS-SIMFIRE-BLAZE[12]	0.5°×0.5°, monthly	2001-2012	GPP, BF

GPP: gross primary productivity; BF: burned fraction, the fraction of burned area within a grid cell (%). Notably another two FireMIP models, LPJ-GUESS-GlobFIRM[13] and MC2[14], were excluded in this study because they provide the yearly burned area datasets.

References

1 Zhang, Y. *et al.* Autumn canopy senescence has slowed down with global warming since the 1980s in the Northern Hemisphere. *Communications Earth & Environment* **4** (2023).

2 Zheng, B. *et al.* Record-high CO2 emissions from boreal fires in 2021. *Science* **379**, 912-917 (2023).

3 Yuan, W. *et al.* Increased atmospheric vapor pressure deficit reduces global vegetation growth. *Science Advances* **5**, eaax1396 (2019).

4 Hantson, S. *et al.* Quantitative assessment of fire and vegetation properties in simulations with fire-enabled vegetation models from the Fire Model Intercomparison Project. *Geoscientific Model Development* **13**, 3299-3318 (2020).

5 Hantson, S. *et al.* Model outputs: Quantitative assessment of fire and vegetation properties in historical simulations with fire-enabled vegetation models from the Fire Model Intercomparison Project [Data set]. *Zenodo* https://doi.org/10.5281/zenodo.3555562 (2019).

6 Li, F., Levis, S. & Ward, D. S. Quantifying the role of fire in the Earth system – Part 1: Improved global fire modeling in the Community Earth System Model (CESM1). *Biogeosciences* **10**, 2293-2314 (2013).

7 Lasslop, G., Thonicke, K. & Kloster, S. SPITFIRE within the MPI Earth system model: Model development and evaluation. *Journal of Advances in Modeling Earth Systems* **6**, 740-755 (2014).

8 Lehsten, V. *et al.* Estimating carbon emissions from African wildfires. *Biogeosciences* **6**, 349-360 (2009).

9 Yue, C. *et al.* Modelling the role of fires in the terrestrial carbon balance by incorporating SPITFIRE into the global vegetation model ORCHIDEE – Part 1: simulating historical global burned area and fire regimes. *Geoscientific Model Development* **7**, 2747-2767 (2014).

10 Melton, J. R. & Arora, V. K. Competition between plant functional types in the Canadian Terrestrial Ecosystem Model (CTEM) v. 2.0. *Geoscientific Model Development* **9**, 323-361 (2016).

11 Mangeon, S. *et al.* INFERNO: a fire and emissions scheme for the UK Met Office's Unified Model. *Geoscientific Model Development* **9**, 2685-2700 (2016).

12 Knorr, W., Jiang, L. & Arneth, A. Climate, CO2 and human population impacts on global wildfire emissions. *Biogeosciences* **13**, 267-282 (2016).

13 Smith, B. *et al.* Implications of incorporating N cycling and N limitations on primary production in an individual-based dynamic vegetation model. *Biogeosciences* **11**, 2027-2054 (2014).

14 Bachelet, D., Ferschweiler, K., Sheehan, T. J., Sleeter, B. M. & Zhu, Z. Projected carbon stocks in the conterminous USA with land use and variable fire regimes. *Glob Chang Biol* **21**, 4548-4560 (2015).